Aerosols: the key to understanding Titan's lower ionosphere

G.J. Molina-Cuberos[a,], S. Cardnell[b], A.J. García-Collado[c], O. Witasse[b], J.J. López-Moreno[d]

[a] *Departamento de Electromagnetismo y Electrónica, Universidad de Murcia, Murcia, Spain.*
[b] *European Space Agency, ESA/ESTEC Scientific Support Office, Directorate of Science, Noordwijk, The Netherlands.*
[c] *Geomática, Teledetección y SIG Aplicados, Universidad Católica de San Antonio, Murcia, Spain.*
[d] *Instituto de Astrofísica de Andalucía, IAA-CSIC, Granada, Spain.*

Abstract

The Permittivity Wave and Altimetry system on board the Huygens probe observed an ionospheric hidden layer at a much lower altitude than the main ionosphere during its descent through the atmosphere of Titan, the largest satellite of Saturn. Previous studies predicted a similar ionospheric layer. However, neither previous nor post-Huygens theoretical models have been able to reproduce the measurements of the electrical conductivity and charge densities reported by the Mutual Impedance (MI) and Relaxation Probe (RP) sensors. The measurements were made from an altitude of 140 km down to the ground and show a maximum of charge densities of $\approx 2\times10^9$ m^{-3} positive ions and $\approx 450 \times 10^6$ m^{-3} electrons at approximately 65 km. Such a large difference between positive and negative charge densities has not yet been understood. Here, by making use of electron and ion capture processes in to aerosols, we are able to model both electron and positive ion number densities and to reconcile experimental data and model results.

Keywords: Titan, Comic Rays, Aerosols, charge concentration, ionosphere

1. Introduction

The atmosphere and surface of Titan, the largest moon of Saturn, was explored by the ESA Huygens Probe in 2005 (*Lebreton et al.*, 2005). During the three hours of descent and surface operations, the probe measured for the very first time the physical properties of its deeper atmosphere and hidden surface. The Permittivity Wave and Altimetry (PWA) subsystem, part of the Huygens Atmospheric Structure Instrument (HASI), determined the atmospheric electrical conductivity by making use of two independent sensors: the Mutual Impedance (MI) and Relaxation Probe (RP) and discovered an ionized layer at approximately 65 km of altitude (*Fulchignoni et al.*, 2005; *Grard et al.*, 2006).

This low ionospheric layer is thought to be produced by cosmic radiation (*Capone et al.*, 1976; *Molina-Cuberos et al.*, 1999b), which is the most penetrating kind of radiation and the only one able to ionize the lower portion of the atmosphere. Cosmic rays ionize the neutral constituents of the atmosphere, producing positive ions and electrons. The PWA data shows that, for example, at the peak of electron density, the concentration of positive ions is approximately four times higher than that of electrons, and the ratio increases with altitude, reaching a factor of approximately 1000 at the top of the sounding range, 140 km (*Hamelin et al.*, 2007; *López-Moreno et al.*, 2008; *Molina-Cuberos et al.*, 2010). In order to explain dissimilar concentrations of electrons and positive ions reported by the PWA sensors in the lower ionosphere, either electrophilic molecular species, embryos or aerosol

particles able to attain negative charge must be considered (*Borucki et al.*, 2006, 2008; *Whitten et al.*, 2007; *Mishra et al.*, 2015).

The existence of an upper ionospheric layer was known since the Voyager 1 flyby (*Bird et al.*, 1997). This layer extends up to approximagely 2200 km altitude (*Galand et al.*, 2014) and it is produced by ultraviolet radiation from the sun on the dayside (*Cravens et al.*, 2005) and energetic particle on the nightside(*Cravens et al.*, 2009). Electrons trapped in the Saturnian magnetosphere can also contribute to the ionization depending on the Saturnian magnetosphere and the Saturn Local time of Titan (*Edberg et al.*, 2015). The dayside electron number densities deduced from the Radio Plasma Wave Science/Langmuir Probe (RPWS/LP) measurements peak at values $\sim 2000 - 5000$ cm^{-3} in the altitude range from 1000 to 1200 km (*Vigren et al.*, 2015), and it results a factor of ~ 2 lower than the values derived in the Cassini multi-instrumental study by *Vigren et al.* (2013).

Titan is the satellite with the densest atmosphere in the Solar System and the only nitrogen-rich atmosphere aside from Earth's. Its atmosphere is mainly composed by nitrogen (97%) and methane (2.7±1%), and lodges trace amounts of a high variety of hydrocarbons such us ethane, diacetylene, methylacetylene, acetylene, and cyanoacetylene (*Niemann et al.*, 2005; *Coustenis and Taylor*, 2008). The atmosphere is characterized by distributed hazes of aerosol layers and the known Titan's orange haze at altitudes of around 500 km (*Israël et al.*, 2005; *Coates et al.*, 2009; *Lavvas et al.*, 2013). Solar radiation and energetic particles coming from the Saturnian magnetosphere dissociate N_2 and CH_4, the major atmospheric constituents, into radicals and ions, which trigger a complex organic chemistry (*Cravens*

et al., 2006; *Magee et al.*, 2009; *Mandt et al.*, 2012) and subsequently leads to the formation of aerosol particles (*Niemann et al.*, 2005; *Coates et al.*, 2009; *Lavvas et al.*, 2013). Those particles can then become charged positively or negatively. At higher altitudes, just below the main ionospheric peak above 950 km, negative and positive molecular ions and predominantly negative charged nm-sized grains have been detected (*Coates et al.*, 2007; *Waite et al.*, 2007; *Shebanits et al.*, 2013, 2016). Several articles have shown the significant role of physical aggregation and ion-neutral chemistry in the production of aerosols (*Sittler et al.*, 2009; *Lindgren et al.*, 2017; *Lavvas et al.*, 2013). It is now widely admitted that studying the ionosphere of Titan at all altitudes cannot be done without considering aerosols.

The models developed before the Huygens arrival predicted that the electron and ion abundances can be affected by attachment to aerosols, during both nighttime and daytime (*Borucki et al.*, 1987, 2006). The post-Huygens models also included other species to decrease the concentration of electrons and to reproduce the observations. *Whitten et al.* (2007) developed a time-dependent model of the nightside ionosphere and found that the electrical charging of aerosol particles is negative and the formation of negative ions is of major importance at night. The presence of a very small abundance (in the range between 10^{-13} and 10^{-11} mole fraction) of electrophilic neutral species in which electrons can be attached by the three-body process and produce negative ions, can reduce appreciably the concentration of electrons below 40 km (*Molina-Cuberos et al.*, 2000).

Borucki et al. (2008) modeled the size and abundance distribution of aerosols by assuming a constant mass flux with altitude and using the re-

ported optical depth at the lower ionosphere by *Tomasko et al.* (2005) as a constraint. Then, the obtained profiles were used to calculate the electron and ion densities and conductivities for varios solar UV photoelectron emission thresholds, because of the Huygens' descent took place during daytime conditions, with a solar zenith angle of around 40°. The comparison with PWA observations indicated that photoemission of electrons cannot be an important source of ionization (*Borucki et al.*, 2008), therefore the structure of the lower ionosphere does not depend on the solar local time. In order to find agreement with observation, they also find that both an additional population of aerosol embryos above 50 km and a very low mole fraction of electrophilic molecules at lower altitudes are needed. Embryos are very small particles ($\approx 7 \times 10^{-4}$ μm) that, at the atmospheric conditions of Titan, can be fullerenes and polycyclic aromatic hydrocarbons (*Sittler et al.*, 2009).

Mishra et al. (2015) solved the state equations for ions and electrons in the presence of aerosols and embryos, allowing both particles to be positively and negatively charged. In order to agree with the observations obtained by the MI sensor (*Hamelin et al.*, 2007), both the concentration of embryos and the photoemission thresholds of aerosols/embryos were adjusted at each altitude. In contrast with *Borucki et al.* (2008), the presence of aerosols increases the conductivity due to electrons and their predictions at 140 km differ approximately by four orders of magnitude with conductivity data retrieved from the RP sensor (*López-Moreno et al.*, 2008; *Molina-Cuberos et al.*, 2010).

In the present work, we take a step forward towards understanding the physical process related with the charge distribution in Titan's atmosphere

below 140 km. *Cardnell et al.* (2016) recently revealed the fundamental role that aerosols play in the photochemistry of the low ionosphere of Mars. Here we follow a similar approach and find that the size and density distribution of aerosols affects the concentration of both positive and negative charge carriers. By making use of electron and ion capture processes onto aerosols and aerosol profiles from Huygens measurements (*Tomasko et al.*, 2008; *Lavvas et al.*, 2010), we are able to reconcile experimental data and model results. We also find that, unlike previous works, no additional population of small embryo particles nor electrophilic neutrals are needed in order to attain a reasonable agreement with the PWA observations.

2. Model

The lower ionosphere of Titan is modeled by considering the balance equations for one kind of cations, electrons and aerosols. A similar treatment was used by *Cardnell et al.* (2016) in the lower Martian ionosphere. Here we make use of the same processes and formulation with the only difference being neglecting electron photodetachment processes (*Borucki et al.*, 2008) due to the large distance to the Sun and the strong absorption of Titan's dense atmosphere (Lara et al., 1996). The photoemision of aerosols was taken into account by *Mishra et al.* (2015) and they found that, in contrast with *Borucki et al.* (2008), the production of electrons by the photoemission of aerosols is an important process, particularly above 80 km. However, the inclusion of this process increases the concentration of electrons and the obtained results disagree with the observations above 80 km.

Transport phenomena can be neglected in the lower atmosphere because

the transport time is several orders of magnitude larger than the chemical lifetime (*Molina-Cuberos et al.*, 1999a). Ions and electrons are produced by cosmic rays and lost by ion-electron recombination and by attachment to aerosols. Assuming steady-state conditions, the continuity equations for positive ions, electrons and aerosols can be written as (*Banks and Kockarts*, 1973):

$$q - \alpha n^+ n^e - \sum_{i=-i_{max}}^{i_{max}-1} \beta_+^i n^+ N^i = 0 \tag{1}$$

$$q - \alpha n^+ n^e - \sum_{i=-i_{max}+1}^{i_{max}} \beta_e^i n^e N^i = 0 \tag{2}$$

$$\beta_+^{i-1} n^+ N^{i-1} + \beta_e^{i+1} n^e N^{i+1} - \beta_+^i n^+ N^{i-1} - \beta_e^i n^e N^i = 0 \tag{3}$$

where n^+ and n^e are the cation and electron number densities, respectively, N^i is the number density of aerosols with i elementary charges, q is the production rate of cations and electrons due to cosmic rays, α the ion-electron recombination coefficient, β_+^i and β_e^i are the attachment coefficients of cations and electrons, respectively, to aerosols with i elementary charges, and $\pm i_{max}$ is the maximum number of elementary charges in an aerosol.

We make use of the atmospheric model reported by *Coustenis and Taylor* (2008) and an adapted cosmic rays spectra for Saturn's orbit and moderate solar activity (*Molina-Cuberos et al.*, 1999b) in order to calculate the ionization rate by cosmic rays. Solar wind interacts with the cosmic particles in the interplanetary medium and its variations related to the solar activity produce changes in the spectrum of cosmic rays. However, due to the long distance to the Sun and the strong absorption of the atmosphere, the effects of the solar conditions on the ionization rate below $\approx$ 150 km are quite low

(*Molina-Cuberos et al.*, 1999b), and, therefore, the results of our model do not depend on the solar activity. The high amount of hydrocarbons and the low temperatures of the atmosphere favour the production of cluster ions (*Capone et al.*, 1976; *Borucki et al.*, 1987; *Molina-Cuberos et al.*, 1999a), which are composed of the electrostatic aggregation of one or several neutral molecules into an ion and recombine with electrons more quickly than the covalently bonded cations. The ion-electron dissociative recombination rates for the most abundant ions are on the form $\alpha_{300} \times (T_e/300)^{\gamma}$, with α_{300} being the rate coefficient at $T_e = 300$ K and with $(T_e/300)^{\gamma}$ describing the electron temperature dependence of the reaction (*Vigren et al.*, 2013). At the lower atmosphere of Titan, the electron temperatature is equal to the atmospheric temperature, T. Experimental values for α_{300} and γ range from 1 to 2 (in $\times 10^{-6}$ cm^3 s^{-1}) and from 0.58 to 0.80, respectively (see *Vigren et al.* (2013) and references therein), here we have adopted a mean rate of $\alpha = 1.5 \times 10^{-6}(300/T)^{0.7}$ cm^3 s^{-1}.

Aerosols can become charged due to ion and electron attachment, both positively and negatively up to several elementary charges. The more negatively charged an aerosol is, the easier it is to capture a positive ion and vice versa. The probability of electrons becoming attached to aerosols is quantified with the electron attachment coefficient *Gunn* (1954):

$$\beta_e^i = \frac{i\mu_e e}{\epsilon_0(1 - exp(-2L))} \tag{4}$$

where i is the number of charges on the aerosol, μ_e the electron mobility, e is the elementary charge, ϵ_0 is the vacuum permittivity, $L = e^2/(8\pi\epsilon_0 a k_B T)$, a is the aerosol radius, and k_B is the Boltzmann constant. *Gunn* (1954) derived the above expression by considering the Coulomb forces at large separations

between a spherical particle carrying i charges and the electron or ion, and by neglecting the induced image charges, which produce short range forces. Since the ionic mean free path is short compared to the aerosol size, we also make use of the method by *Gunn* (1954) to model the ion attachment to aerosol particles. This approximation is not applicable within the low collisional regime of the upper ionosphere. Aerosols are allowed to become charged up to $\pm i_{max}$ elementary charges, which give rise to $2i_{max}+1$ aerosol balance equations. The maximum positive and negative charge the aerosols are allowed to attain is set at $i_{max} = 150$, which was twice the minimum value required to adequately represent the aerosol charge distribution.

The distribution of aerosols strongly affects the density of positive ions and electrons. In the present work, the two aerosol density profiles reported by *Tomasko et al.* (2008), with a constant aerosol size of 720 μm, where used, see Fig. 1. These profiles were obtained using measurements from the two channels of the solar aureole (SA) instrument onboard Huygens, corresponding to the 491 and 934 nm wavelengths (*Tomasko et al.*, 2008). The results agree above 80 km, but differ sightly below this altitude. More recently, *Lavvas et al.* (2010) presented a one dimension study of Titan's aerosol distribution. They considered a constant mass production of aerosols in the thermosphere to 3×10^{-14}g cm^{-2} s^{-1} and modelled the evolution of the particles due to coagulation, sedimentation and atmospheric mixing. *Lavvas et al.* (2010) obtained a lower number density and an aerosol size of 850 μm, that can be considered constant at the altitude range of Hyugens, also plotted in Fig. 1.

The aerosol charging processes do not alter the total aerosols number

density, N:

$$N = \sum_{i=-i_{max}}^{i_{max}} N^i \tag{5}$$

The condition of charge neutrality requires that:

$$\sum_{i=-i_{max}}^{i_{max}} iN^i + n^+ - n^e = 0 \tag{6}$$

The concentration of cations, electrons and charged aerosols were calculated by solving the system of algebraic equations (1)-(5), and using the *fsolve* function provided by Matlab^{TM}. This technique iteratively minimizes the sum of squares of the components from an initial guess and a range of initial guess values were tested to ensure the final results. Once the charge concentrations are calculated, the mobilities due to positive ions and electrons are used to calculate the two branches of electrical conductivity, corresponding to the positive and negative charges. Assuming that electrons mainly collide with molecular nitrogen, the electron mobility can be derived as follows (*Banks and Kockarts*, 1973):

$$\mu^e = \frac{e}{2.33 \times 10^{-17} N_n T} \tag{7}$$

where μ^e is given in $m^2\ s^{-1}\ V^{-1}$ and N_n the neutral number density in m^{-3}. The ionic mobility depends on the ionic mass. Here we make use of a functional equation (*Meyerott et al.*, 1980):

$$\mu^+ = \frac{T}{273}\frac{101325}{P}\left[\left(\frac{850}{m^+}\right)^{1/3} - 0.3\right] \cdot 10^{-4} \tag{8}$$

where P the pressure in Pa and the ionic mass m^+ is expressed in amu. Numerical models predict a mean ionic mass in the range between 50 and

150 amu (*Molina-Cuberos et al.*, 1999a), although more massive ions are not excluded. Here, we make use of a mean value of $m^+ = 100$ amu.

3. Results and Discussion

Figure 2 compares the two components of the electrical conductivity results with our model and the measurements obtained from the RP and MI data. The RP technique allows differentiation between the conductivity due to positive and negative charges and, therefore, can provide information about the densities of both charge carriers (*López-Moreno et al.*, 2008; *Molina-Cuberos et al.*, 2010). However, this method requires long time periods, which decreases the spatial resolution. In contrast, the MI technique is only sensitive to the total electrical conductivity and has a faster measurement rate (*Hamelin et al.*, 2007).

The RP provided the conductivity due to positive ions above approximately 65 km; below this altitude the relaxation time was too long to be measured (*López-Moreno et al.*, 2008). We observe that the calculated conductivities are very similar for the three analyzed aerosol profiles. We have found a very good agreement with experimental results and does not differ too much from the results of the model not considering aerosols (also plotted in Fig 2).

The most important improvement of this model is the resulting conductivity due to electrons. Without taking into account the role of aerosols (non-aerosol case in Fig 2), the results show a very good agreement below the peak at approximately 60 km. However, above this maximum, while the non-aerosol model predicts an increase in conductivity with altitude, the

measurements indicate an exponential decrease, reaching a disagreement of four orders of magnitude at 140 km. We observe that the inclusion of aerosols in the model strongly reduces the conductivity due to electrons, mainly at higher altitudes, and allows the convergence between model results and experimental measurements. The best agreement is found with the aerosol profile retrieved from the 930 nm channel, in fact, calculations also reproduce the observed small decrease at around 80 km. MI reported conductivity measurements down to the ground (*Hamelin et al.*, 2007). However, the authors intentionally limited the density profile to an altitude of 40 km because of the lack of accuracy as the conductivity decreases. Our results also agree with the MI data, even at this altitude range, which may also support the measurements obtained by MI.

Figure 3 shows the densities of positive ions and electrons obtained by our model and the retrieved ones from the RP and MI measurements. The electron density, which obviously coincides with the positive ion density for the non-aerosol case, is also plotted. The error bars associated with the concentration of positive ions take into account the errors in the numerical fitting and the uncertainties of the ionic mass (*López-Moreno et al.*, 2008). Again, we observe a very good agreement between model predictions and the densities obtained from conductivity measurements. The presence of aerosols reduces the concentration of both electrons and ions. The decrease in the concentration of electrons is much greater and, therefore, the concentration of electrons is not equal to that of positive ions, which means that an important amount of negative charge is accumulated on aerosols (Fig 4). In fact, the amount of negative charge attached onto aerosols is similar to the

number of electrons. The ratio ions/electrons decreases with altitude, from approximately 350 at the top of our altitude range to a minimum of approximately 1.1 at ≈ 70 km, then it remains almost constant down to the ground, where the concentration of positive charge is twice that of electrons. Both electrons and positive ions peak at approximately 62 km, roughly the same altitude where ionization rate peaks (65 km).

Figure 4 shows the distribution of charged aerosols obtained in our simulation. Aerosols tend to become negatively charged due to the more efficient attachment of electrons than that of positive ions. The mean number of electrons attached to aerosol particles depends on altitude and is in the range between 30 and 50. Electron trapping in aerosols leads to $\approx$ 60 charges/radius (in μm), which is between the results obtained in tholin material, 628 charges/radius for Titan-like aerosols particles by *Pirim et al.* (2015) and the 7.5 charges/radius used by *Larson et al.* (2014) in a three dimensional general circulation model with microphysics treatment of aerosols. At the maximum of the electron concentration, approximately 60 km, aerosol particles lodge approximately 30 electrons and close to the surface slightly more, approximately 35 electrons. The charged aerosol number density increases with altitude from the ground up to approximately 40 km, where it peaks at approximately 1.4×10^6 m^{-3} and then decreases.

4. Conclusions

The lower ionosphere of Titan has been modeled and the electrical conductivity due to positive charges and electrons was calculated in order to reconcile the experimental data obtained by the PWA system on board the

Huygens probe. The main conclusions obtained in this work are as follows:

1. The presence of aerosols reduces the values of the two components of the electrical conductivity. The used aerosol profile allows to reconcile the model results with the experimental measurements obtained both by the MI and the RP sensors in the whole altitude range, from 140 km down to the ground.

2. The inclusion of aerosols decreases the concentration of both electrons and ions. This reduction is greater for the case of electrons and, therefore, the concentration of electrons is not equal to that of positive ions. The ratio ions/electrons decreases with altitude, from ≈ 350 at 140 km to a minimum of ≈ 1.1 at ≈ 70 km.

3. Both electrons and positive ions peak at ≈ 62 km, roughly the same altitude where ionization rate peaks (65 km).

4. Aerosols are negatively charged and the main number of electrons attached to aerosol particles is in the range between 30 and 50.

Acknowledgments

The authors thank Panayotis Lavvas for his suggestions and comments. This work was supported by the Spanish Government (Project TEC2014-55463-C3-1-P) and by the European Commission (ERDF). O. Witasse and S. Cardnell acknowledge the ESA Young Graduate Trainee program.

References

Banks, P. M., and Kockarts, G. (1973), *Aeronomy, vol. 2* Academic Press, New York.

318 Bird, M. K., Dutta-Roy, R., Asmar, S. W., et al. (1997), Detection of Titan's
319 Ionosphere from Voyager 1 Radio Occultation Observations, *Icarus 130(2),*
320 426–436.

321 Borucki, W. J., Levin, Z., Whitten, R. C., et al (1987), Predictions of the
322 electrical conductivity and charging of the aerosols in Titan's atmosphere,
323 *Icarus 72,* 604 – 622.

324 Borucki, W. J., Whitten, R. C., Bakes, E. L. O., et al. (2006), Predictions
325 of the electrical conductivity and charging of the aerosols in Titan's atmo-
326 sphere, *Icarus 181,* 527 –544.

327 Borucki, W. J., and Whitten, R. C. (2008), Influence of high abundances of
328 aerosols on the electrical conductivity of the Titan atmosphere, *Planetary*
329 *and Space Sci. 56,* 19 –26.

330 Capone, L. A., Whitten, R. C., Dubach, J., Prasad, S. S., and Huntress,
331 W. T., Jr. (1976), The lower ionosphere of Titan, *Icarus 28,* 367 –378.

332 Cardnell, S., Witasse, O., Molina-Cuberos, G. J., et al. (2016), A photochem-
333 ical model of the dust-loaded ionosphere of Mars, *Journal of Geophysical*
334 *Research (Planets) 121,* 2335 –2348.

335 Coates, A. J., Crary, F. J., Lewis, G. R., et al. (2007), Discovery of heavy
336 negative ions in Titans ionosphere, *Geophys. Res. Lett. 34(22),* L22103.

337 Coates, A. J., Wellbrock, A., Lewis, G. R., et al. (2009), Heavy negative ions
338 in Titan's ionosphere: Altitude and latitude dependence, *Planet. Space*
339 *Sci. 57(14-15),* 1866–1871.

340 Cravens, T. E., Robertson, I. P., Clark, J., et al. (2005), Titan's ionosphere:
341 Model comparisons with Cassini Ta data, *Geophys. Res. Lett. 32(12),*
342 L12108.

343 Cravens, T. E., Robertson, I. P., Waite, J. H., et al. (2006), Composition of
344 Titan's ionosphere, *Geophys. Res. Lett. 33(7),* L07105.

345 Cravens, T. E., Robertson, I. P., Waite, J. H., et al. (2009), Model-data
346 comparisons for Titans nightside ionosphere, *Icarus 199(1),* 174188.

347 Coustenis, A., and Taylor, F. W. (2008), *Titan: Exploring an Earthlike*
348 *World,* World Scientific, Singapure.

349 Edberg, N. J. T., Andrews, D. J., Bertucci, C., et al. (2015), Effects of
350 Saturn's magnetospheric dynamics on Titan's ionosphere, *J. Geophys. Res.*
351 *Sp. Phys. 120(10),* 8884-8898.

352 Fulchignoni, M., Ferri, F., Angrilli, F., et al. (2005), In situ measurements of
353 the physical characteristics of Titan's environment, *Nature 438,* 785 –791.

354 Galand, M., Coates, A. J., Cravens, T. E., et al. (2014), Titan's ionosphere,
355 in *Titan*, edited by Muller-Wodarg, I., Griffith, C. A., Lellouch, E., and
356 Cravens, T. E., 376–418, Cambridge University Press, Cambridge.

357 Grard, R., Hamelin, M., López-Moreno, J. J., et al. (2006), Electric proper-
358 ties and related physical characteristics of the atmosphere and surface of
359 Titan, *Planetary and Space Science 54,* 1124 –1136.

360 Gunn, R. (1954), Diffusion charging of atmospheric droplets by ions, and the

361 resulting combination coefficients, *Journal of Atmospheric Sciences 11*(5)
362 339–347.

363 Hamelin, M., Béghin, C., Grard, R., et al. (2007), Electron conductivity and
364 density profiles derived from the mutual impedance probe measurements
365 performed during the descent of Huygens through the atmosphere of Titan,
366 *Planetary and Space Science 55,* 1964 –1977.

367 Israël, G., Szopa, C, Raulin, F., et al. (2005), Complex organic matter in
368 Titan's atmospheric aerosols from in situ pyrolysis and analysis, *Nature*
369 *438,* 796 –799.

370 Lavvas, P., Yelle, R. V., and Griffith, C. A. (2010), Titans vertical aerosol
371 structure at the Huygens landing site: Constraints on particle size, density,
372 charge, and refractive index, *Icarus 210,* 832 – 842.

373 Lavvas. P., Yelle, R. V., Koskinen, T. et al. (2013), Aerosol growth in Titans
374 ionosphere, *Proc Natl Acad Sci USA 110,*, no. 8, 2729–2734.

375 Lara, L. M., Lellouch, E., López-Moreno, J. J., et al. (1996), *Journal Geo-*
376 *phys. Res. 101,* 23261.

377 Larson, E., Owen, T. B., and Friedson, J. A., (2014), Simulating Titans
378 aerosols in a three dimensional general circulation model, *Icarus 243,* 400
379 – 419.

380 Lebreton, J.-P., Witasse, O., Sollazzo, C., et al. (2005), An overview of the
381 descent and landing of the Huygens probe on Titan, *Nature 438,* 758 –764.

Lindgren, E. B., Stamm B., Chan H.-K., et al. (2017), The effect of like-charge attraction on aerosol growth in the atmosphere of Titan, *Icarus 291,* 245–253.

López-Moreno, J. J., Molina-Cuberos, G. J., Hamelin, M., et al. (2008), Structure of Titan's low altitude ionized layer from the Relaxation Probe onboard HUYGENS, *Geophysical Research Letters 35,* L22104.

Magee, B. A., Waite, J. H., Mandt, K. E., et al. (2009), INMS-derived composition of Titan's upper atmosphere: Analysis methods and model comparison, *Planet. Space Sci. 57(14-15),* 1895–1916.

Mandt, K. E., Gell, D. A., Perry, M., et al. (2012), Ion densities and composition of Titan's upper atmosphere derived from the Cassini Ion Neutral Mass Spectrometer: Analysis methods and comparison of measured ion densities to photochemical model simulations, *J. Geophys. Res. 117(E10),* E10006.

Meyerott, R. E., Reagan, J. B., and Joiner, R. G. (1980), The mobility and concentration of ions and the ionic conductivity in the lower stratosphere, *Journal of Geophysical Research 85,* 1273 –1278.

Mishra, A., Michael, M., Tripathi, S. N., and Béghin, C. (2014), Revisited modeling of Titan's middle atmosphere electrical conductivity, *Icarus 238,* 230 –234.

Molina-Cuberos, G. J., López-Moreno, J. J., Rodrigo, R., and Lara, L. M. (1999a), Chemistry of the galactic cosmic ray induced ionosphere of Titan, *Journal of Geophysical Research 104,* 21997 –22024.

405 Molina-Cuberos, G. J., López-Moreno, J. J., Rodrigo, R., Lara, L. M., and
406 O'Brien, K. (1999b), Ionization by cosmic rays of the atmosphere of Titan,
407 *Planetary and Space Science 47,* 1347 –1354.

408 Molina-Cuberos, G. J., López-Moreno, and J. J., Rodrigo (2000), Influence
409 of Electrophilic Species on the Lower Ionosphere of Titan, *Geophysical*
410 *Research Letters 27 (9)* 1351–1354.

411 Molina-Cuberos, G. J., Godard, R., López-Moreno, J. J., et al. (2010), A
412 new approach for estimating Titan's electron conductivity based on data
413 from relaxation probe sensors on the Huygens experiment, *Planetary and*
414 *Space Science 58,* 1945 –1952.

415 Niemann, H. B., Atreya, S. K., Bauer, S. J., et al (2005), The abundances
416 of constituents of Titan's atmosphere from the GCMS instrument on the
417 Huygens probe, *Nature 438(7069),* 779–784.

418 Pirim, C., Gann, R. D., McLain, J. L., et al. (2015), Electron-molecule chem-
419 istry and charging processes on organic ices and Titan's icy aerosol surro-
420 gates, *Icarus 258,* 109 – 119.

421 Shebanits, O., Wahlund, J.-E., K. Mandt, K., et al. (2013), Negative ion den-
422 sities in the ionosphere of TitanCassini RPWS/LP results, *Planet. Space*
423 *Sci. 84,* 153–162.

424 Shebanits, O., Wahlund, J.-E., Edberg, N. J. T., et al. (2016), *J. of Geophys.*
425 *Res (Space Physics) 121,* 10.

426 Sittler, E. C., Ali, A., Cooper, J. F., et al. (2009), Heavy ion formation

427 in Titan's ionosphere: Magnetospheric introduction of free oxygen and a
428 source of Titan's aerosols?, *Planetary and Space Science 57,* 1547 –1557.

429 Tomasko, M. G., Archinal, B., Becker, T., et al. (2005), Rain, winds and
430 haze during the Huygens probe's descent to Titan's surface, *Nature 438,*
431 765 – 778.

432 Tomasko, M. G., Doose, L., Engel, S., et al. (2008), A model of Titan's
433 aerosols based on measurements made inside the atmosphere, *Planetary*
434 *and Space Science 56,* 669 –707.

435 Vigren, E., Galand, M., Yelle, R.V., et al., (2013), On the thermal electron
436 balance in Titan's sunlit upper atmosphere. *Icarus 223,* 234–251.

437 Vigren, E., Galand, M., Yelle, R. V., et al., (2015), Ionization balance in
438 Titan's nightside ionosphere, *Icarus 248,* 539–546.

439 Waite, J. H., Young, D. T., Cravens, T. E., et al.(2007), The process of tholin
440 formation in Titan's upper atmosphere, *Science 316(5826),* 870–875.

441 Whitten, R. C., Borucki, W. J., Tripath, S. (2007), Predictions of the electri-
442 cal conductivity and charging of aerosols in Titan's nighttime atmosphere,
443 *Journal of Geophysical Research 112,* E04001.

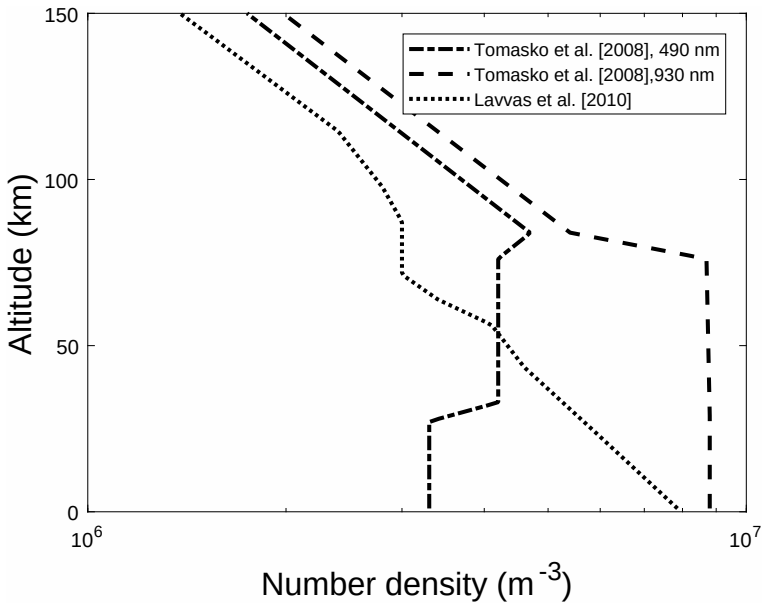

Figure 1: Aerosol number density as a function of altitude for the three diffent models used in this paper. All the models were developed for the Titan conditions during the descent of Huygens, same as the present model.

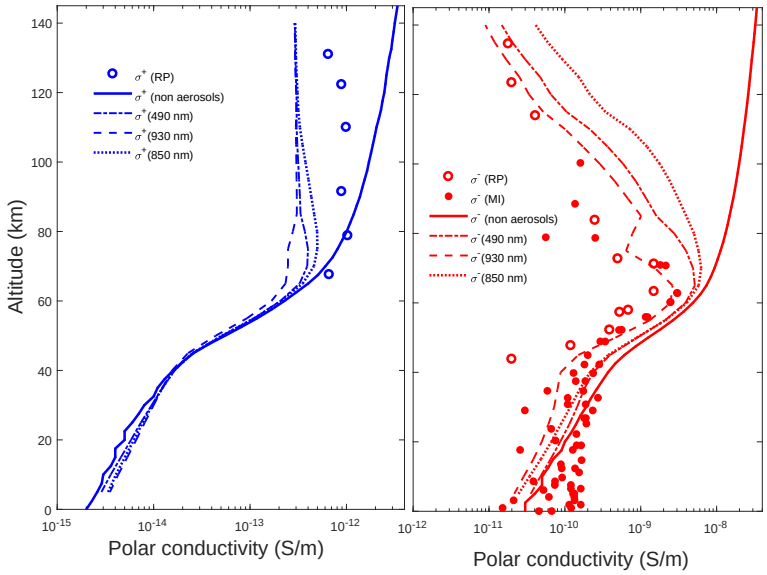

Figure 2: Electrical conductivity due to positive (left panel) and negative charges (right panel), where the symbols are for MI and RP measurements (*Hamelin et al.*, 2007; *López-Moreno et al.*, 2008; *Molina-Cuberos et al.*, 2010), solid line for the non-aerosol case and the other lines for the aerosol number densities shown in Fig. 1.

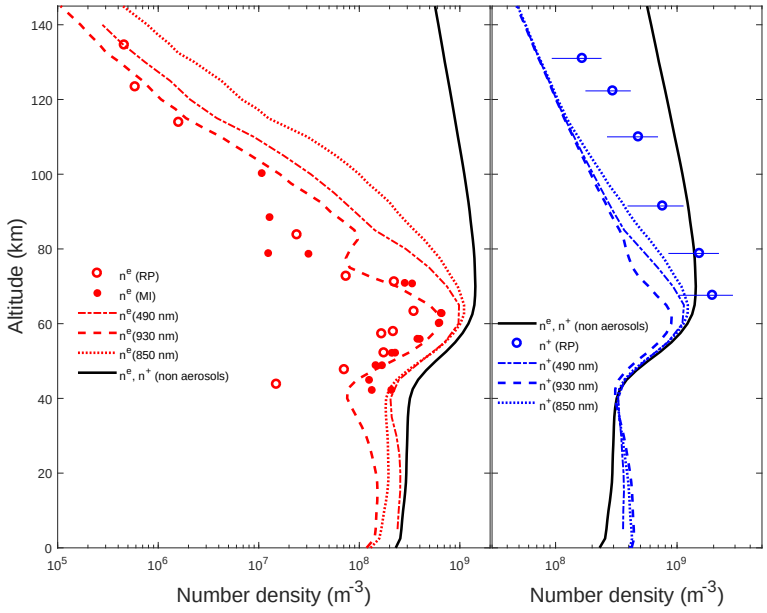

Figure 3: Calculated electron (left panel) and ion (right panel) densities (lines) and retrieved from MI and RP measurements (symbols).

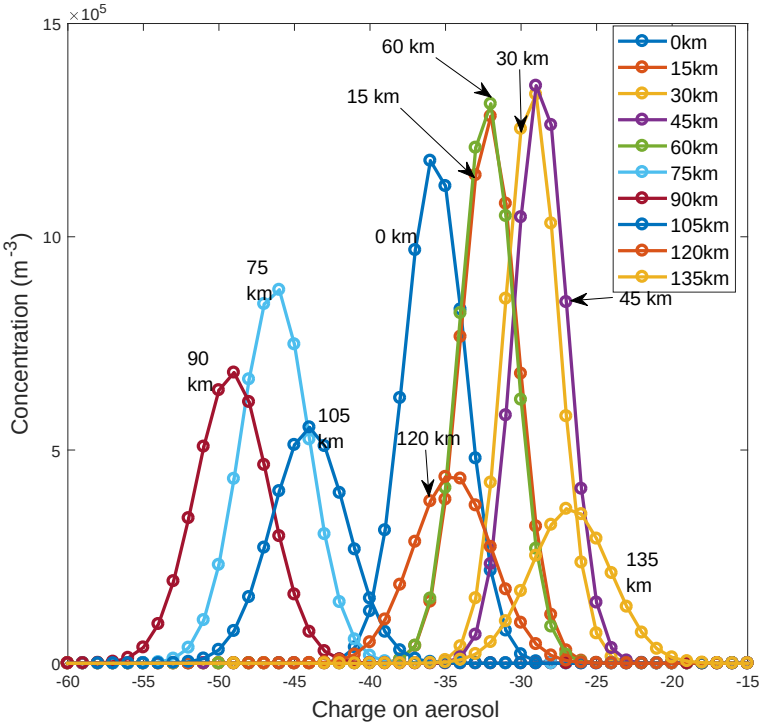

Figure 4: Distribution of charges on aerosols at various altitudes, the aerosol number density profile is from *Tomasko et al.* (2008) 930 nm, Fig. 1.